Earth, Planets and Space

FULL PAPER Open Access

Atmospheric modes excited by the 2021 August eruption of the Fukutoku-Okanoba volcano, Izu–Bonin Arc, observed as harmonic TEC oscillations by QZSS

Kosuke Heki* and Tatsuya Fujimoto

Abstract

Continuous Plinian eruptions of volcanoes often excite atmospheric resonant oscillations with several distinct periods of a few minutes. We detected such harmonic oscillations by the 2021 August eruption of the Fukutoku-Okanoba volcano, a submarine volcano in the Izu–Bonin arc, in ionospheric total electron content (TEC) observed from Global Navigation Satellite System (GNSS) stations deployed on three nearby islands, Chichijima, Hahajima, and Iwojima. Continuous records with the geostationary satellite of Quasi-Zenith Satellite System (QZSS) presented four frequency peaks of such atmospheric modes. The harmonic TEC oscillations commenced at ~5:16 UT with a large amplitude but decayed in a few hours.

Keywords: QZSS, GNSS, Ionospheric disturbance, Total electron content, Fukutoku-Okanoba, Plinian eruption, Atmospheric mode

*Correspondence: heki@sci.hokudai.ac.jp
Department of Natural History Science, Hokkaido University, Sapporo, Japan

Graphical Abstract

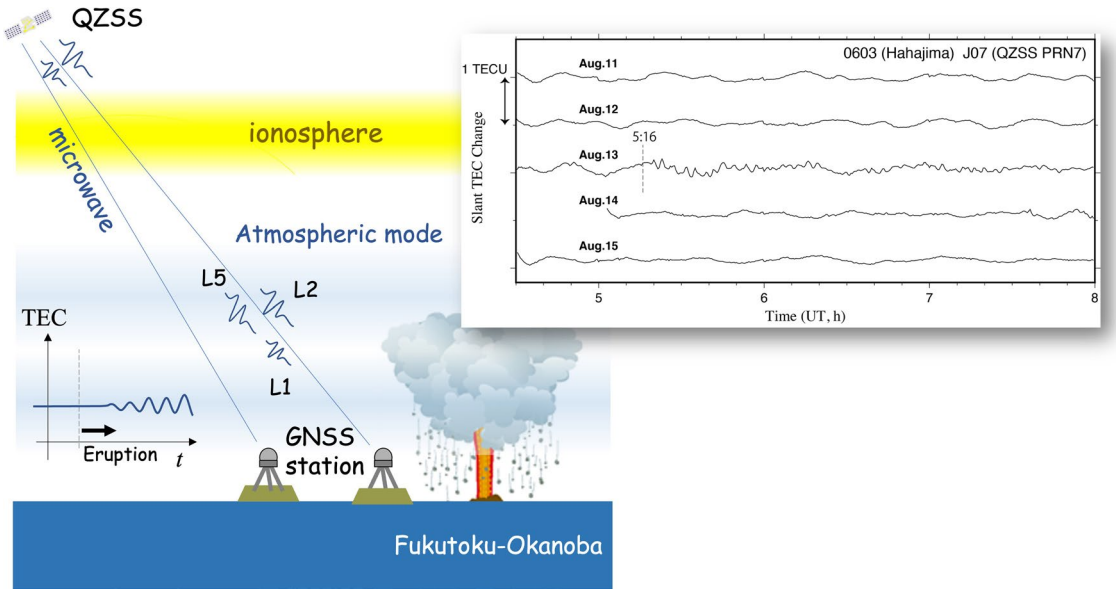

Introduction

With arrays of continuous Global Navigation Satellite System (GNSS) stations, we can continuously monitor the Earth's ionosphere in terms of total electron content (TEC), an integrated number of electrons along line-of-sights connecting satellites and receivers. GNSS-TEC observations enabled us to detect ionospheric responses to large volcanic eruptions worldwide during the last two decades. Such responses have two distinct types (Type-1) harmonic oscillations of TEC (e.g., Nakashima et al. 2016), and (Type-2) short pulses of TEC changes (e.g., Heki 2006). Type-1 disturbances are caused by continuous Plinian eruptions and often last for hours. Type-2 disturbances occur 8–10 min after Vulcanian explosions of volcanoes as single N-shaped changes of TEC. Both types propagate outward with a speed of 0.8–1.0 km/s, the acoustic wave velocity in the ionospheric F region. Cahyadi et al. (2020) and Cahyadi et al. (2021) compiled the recent cases of such Type-1 and Type-2 disturbances, respectively. Type-1 cases have never been found in Japan except the 2009 eruption signal of the Sarychev Peak Volcano, Russia, from stations in northern Japan (Shestakov et al. 2021).

Global Positioning System (GPS) has been the main GNSS used to study ionospheric TEC. GPS satellites employ orbits with periods of a half sidereal day and can stay within the view of a ground station only for periods shorter than 4–5 h. On the other hand, Quasi-Zenith Satellite System (QZSS), the Japanese satellite system for positioning, is composed of three satellites with quasi-zenith orbits (J01, J02, J03) and one geostationary orbit satellite (J07). These satellites stay longer within the view of a station (~8 and 24 h a day for J01-03 and J07, respectively). This offers a rare opportunity to observe the TEC oscillation caused by a Plinian volcanic eruption lasting for hours without disruptions of data. In this study, we take this advantage in discussing the frequency content and temporal decay of the oscillation caused by a recent Type-1 ionospheric disturbance case by a volcanic eruption in Japan.

Ionospheric response to the 2021 August eruption of the Fukutoku-Okanoba volcano

The 2021 Plinian eruption

Fukutoku-Okanoba is a submarine volcano located ~5 km NNE of Kita-Iwojima Island (uninhabited) in the Izu–Bonin arc, located ~1000 km south of Tokyo, Japan (Fig. 1). Its submarine eruptions in 1904–1905, 1914, and 1986 resulted in formation of a tiny island, which disappeared within a few years by collapse and marine erosion.

The latest volcanic activity started in 2020 February, when the sea water of this area changed its color to yellow-green. A strong eruption with Volcanic Explosivity Index (VEI) 4 started on August 13, 2021. According to Japan Meteorological Agency (JMA), the eruption column as high as ~16,000 m lasted from August 13, 00 UT to August 14, 19 UT (JMA 2021).

Formation of an island with a diameter of ~1 km was confirmed on August 15, but this new island has been shrinking day by day. The 2021 eruption is one of the

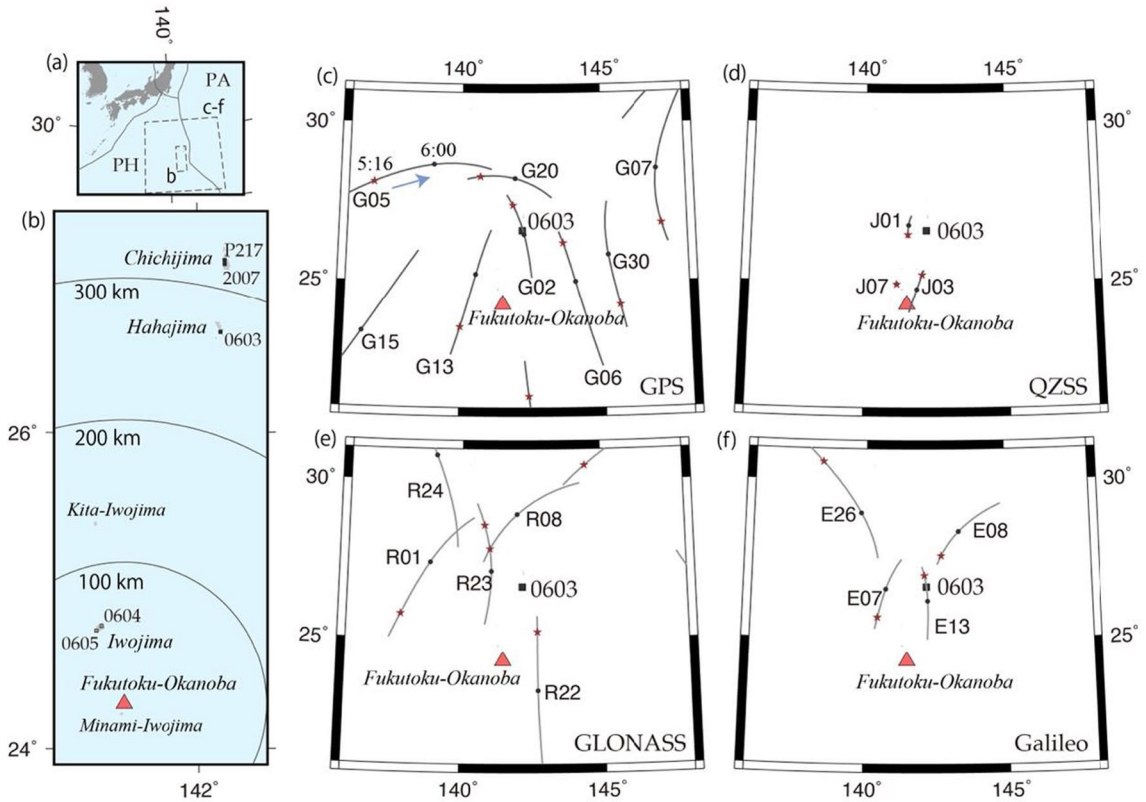

Fig. 1 A map **a** showing the boundaries of the Pacific (PA) and the Philippine Sea (PH) Plates and the coverages of the other maps. **b** Shows the locations of the volcano Fukutoku-Okanoba, which erupted in 2021 August, and three islands, Iwojima, Hahajima, and Chichijima, where five GEONET stations are deployed. Maps in **c–f** show sub-ionospheric point (SIP) tracks 5.1–6.9 UT calculated assuming a thin ionosphere at 300 km altitude for the pairs of the station 0603 and four different GNSS, GPS (**c**), QZSS (**d**), GLONASS (**e**), and Galileo (**f**). Red stars and black circles on the trajectories show time marks of the onset (5:16 UT) of the oscillation and 6:00 UT. A satellite SIP therefore moves in the direction from the red star toward the black circle

largest eruptions in Japan in terms of the total mass of the ejecta. A few months later, huge amount of floating pumice reached the coast of the Ryukyu Islands, southwestern Japan, hindering fishing and ferry navigation in that region.

Eruption signatures in GNSS-TEC

We use GNSS raw data files from GEONET (GNSS Earth Observation Network) run by Geospatial Information Authority (GSI), Japan. Within ~300 km from the Fukutoku-Okanoba volcano, there are five GEONET stations on three inhabited islands, P217 and 2007 on Chihijima, 0603 on Hahajima, and 0604 and 0605 on Iwojima (Fig. 1b). Although the two stations in Iwojima track only GPS satellites, the three other stations track GLONASS, Galileo, and QZSS in addition to GPS. Figure 1c–f shows sub-ionospheric point (SIP) trajectories of these four GNSS as viewed from 0603, Hahajima. SIP trajectories of the QZSS satellites are much shorter than other GNSS, and the SIP of J07 hardly moves. This indicates that these satellites are nearly fixed in the sky when viewed from the ground station.

We converted the L1 and L2 carriers into total electron contents (TEC) (we also try L5 as discussed later in this article). Basic procedures in the GNSS-TEC studies follow Heki (2021). Figure 2 compares the TEC time series 4:30–8:00 UT obtained using the QZSS geostationary satellite (J07) from the 0603 station over five consecutive days, August 11–15, 2021. Geomagnetic activities during this period were calm, and the daily *Kp* index remained within the range 0.7–2.0 (omniweb.gsfc.nasa.gov). Clear TEC oscillation started at ~5:20 UT on August 13, the day the Plinian eruption started. This is a typical ionospheric signature of Plinian volcanic eruptions (Cahyadi et al. 2020). Such oscillations are not seen on other days.

In Fig. 3a, we selected stations 2007, 0603, 0605 representing the three islands, Chichijima, Hahajima, and Iwojima, respectively, and showed slant TEC time series on Aug. 13, 2021, using various GNSS satellites with SIP located close to the volcano. Those observed at P217

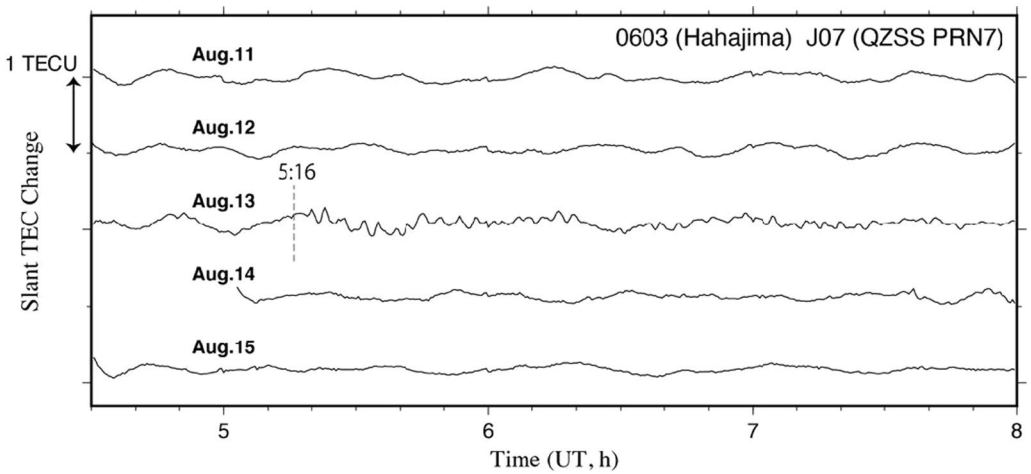

Fig. 2 Slant TEC time series at 0603 with J07 satellite 4:30–8:00 UT on 5 days, August 11–15, 2021. They are high-pass filtered by taking residuals from best-fit degree 9 polynomials. A typical Plinian eruption signature (TEC oscillation with period ~4 min) is seen after 5 UT only on August 13, the starting day the Plinian eruption. The unit TECU (TEC unit) indicates 10^{16} electrons/m^2

and 0604 are not shown because they are very similar to those at 2007 and 0605 stations, respectively. In Fig. 3b, we modified the time axis correcting for the travel time of the acoustic wave from the volcano to the ionospheric penetration points of line-of-sights assuming 0.8 km/s propagation velocity observed in past cases (Nakashima et al., 2016; Kundu et al. 2021). We can see that the phases of TEC oscillations are largely coherent among different satellite–station pairs and that the atmospheric oscillation started at around 5:16 right above the volcano.

Outward propagation of ionospheric disturbances from the volcano can be confirmed also in Fig. 4, where we plot the disturbances observed by various station–satellite pairs in colors as functions of time (horizontal axis) and distance from the volcano (vertical axis). There, we can recognize peaks align along lines with a slope corresponding to the assumed acoustic wave speed (0.8 km/s).

Discussion and conclusion

Frequency spectra of the TEC oscillations

The amplitudes of the TEC oscillation (Fig. 3) vary in time, possibly by the interference of oscillations in multiple frequency peaks. Long continuous TEC records enabled by QZSS are suitable for studying their frequency spectra. Figure 5a shows the time series of slant TEC of J07 observed at three stations (0603 on Hahajima, 2007 and P217 on Chichijima) in 5:00–9:30 UT. A positive pulse at ~ 8:50 UT observed at 2007 and P217 would possibly be a sporadic-E irregularity (e.g., Maeda and Heki 2015) irrelevant to the volcanic eruption. We select the 4-h data 5:20–9:20 and estimated their frequency components using the Blackman–Tukey method (Fig. 5b).

They show four frequency peaks at about 3.7, 4.4, 4.8, and 5.4 mHz, with the 4.8 mHz peak weaker than the other three. The power shows a sharp drop for frequencies lower than 3.7 mHz possibly because this frequency is close to the acoustic cut-off of the atmospheric filter (Blanc 1985). These frequencies correspond to periods of about 270, 227, 208, and 185 s, respectively. The first two are the atmospheric resonance frequencies detected by seismometers after the 1991 eruption of the Pinatubo volcano (e.g., Kanamori and Mori 1992). They also coincide with the two modes with abnormally large amplitudes in the background free oscillation of the Earth (Nishida et al. 2000). The higher two frequencies are also overtones of the atmospheric resonant oscillation (Watada and Kanamori 2010).

These frequencies would depend on local atmospheric structures such as the mesopause altitudes. Precise identification of these peaks is important to investigate differences in atmospheric structures. We emphasize the benefit of long arcs enabled by QZSS because such a study would have been difficult with short arcs of conventional GNSS like GPS.

Temporal decay of the TEC oscillations

Next, we analyze how such TEC oscillation decayed in time. Figure 6a compares time series in two sequential 3-h periods (5:20–8:20 and 8:20–11:20) and two spectrograms made using the initial 2 hours of these time windows. Strong atmospheric mode peaks in the earlier time disappear in the later time (Fig. 6b). Figure 6c shows gradual decay of the three peak frequency intensities. Because the time corresponds to local afternoon (5:20 UT is 14:20 in the local time), background TEC

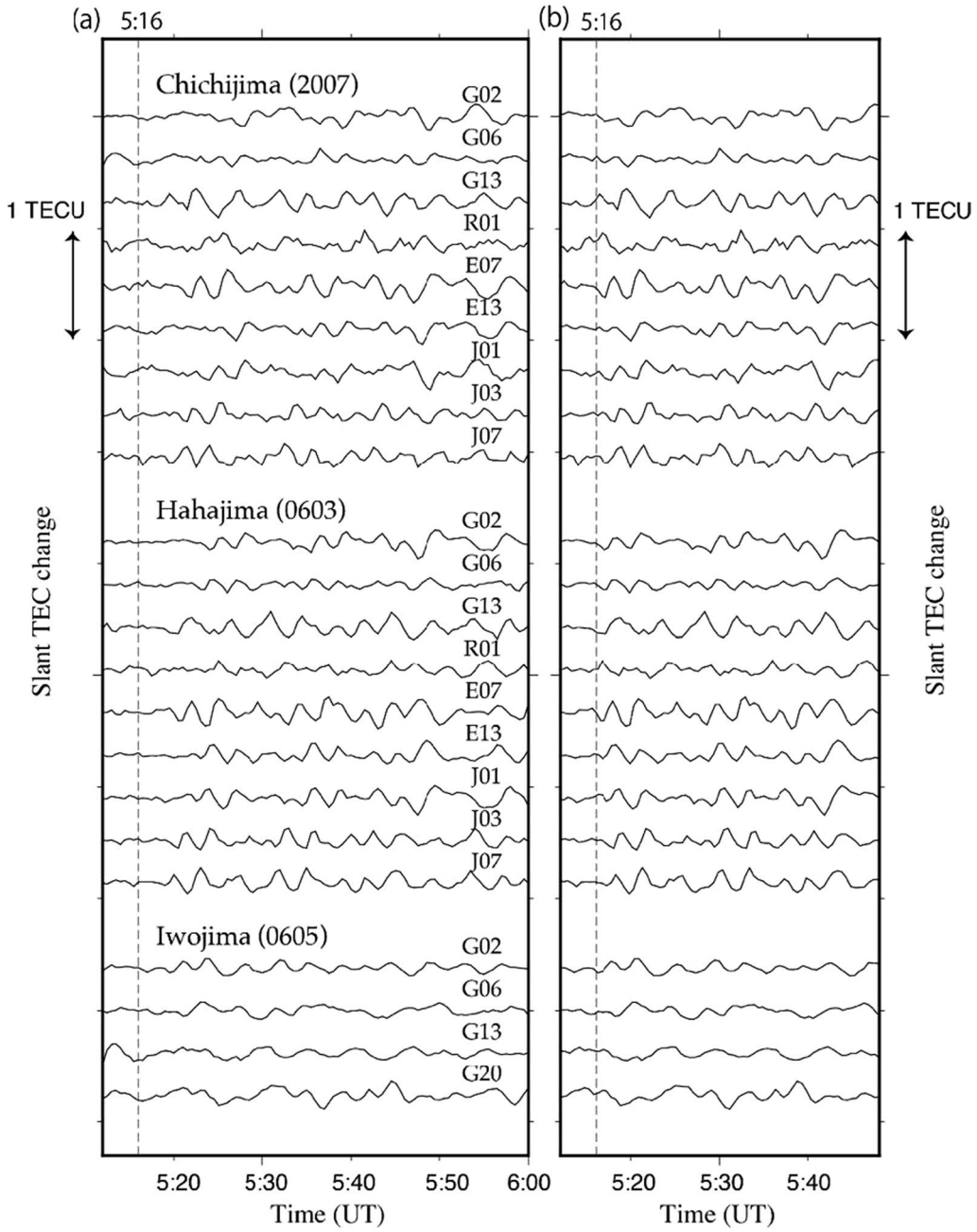

Fig. 3 **a** High-pass filtered slant TEC time series with various combinations of three stations and satellites of four different GNSS (G, R, E, J indicates GPS, GLONASS, Galileo, and QZSS, respectively). In **b**, we corrected for the travel time of acoustic wave assuming the propagation velocity of 0.8 km/s and time-variable distances between the volcano and ionospheric piercing points of line-of-sights (altitude assumed as 300 km), to reproduce hypothetical oscillation signals right above the volcano

also decays. However, the decay of the oscillation exceeds that in the background TEC calculated with a global ionospheric map (GIM) (Mannucci et al. 1998) suggesting that the atmospheric resonance would have decayed substantially within 3 h (Fig. 6c). We consider this decay reflects that of the excitation source (the Plinian eruption itself) rather than the diminishing of the oscillation governed by its quality factor.

Comparison of 3 different combinations of L1, L2, and L5

The QZSS satellites transmit microwave signals in three different frequencies L1 (~ 1.575 GHz), L2

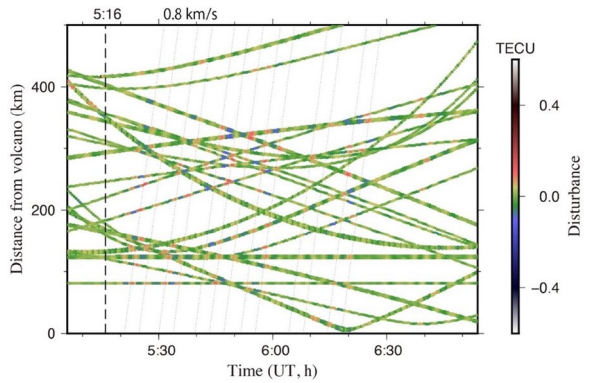

Fig. 4 Short period TEC disturbances (positive/negative changes expressed in red/blue) as functions of time (horizontal axis) and the distance from the Fukutoku-Okanoba volcano (vertical axis) for all the satellite–station pairs showing the eruption signatures. Thin lines, connecting points of clear positive anomalies, have a slope corresponding to the acoustic wave propagation speed (0.8 km/s)

(~1.228 GHz), and L5 (~1.176 GHz). So far, we have been combining L1 and L2 phases to calculate TEC, but the three frequencies allow us to compare three different combinations (L1–L2, L1–L5, and L2–L5) for TEC. Let f_h and f_l be the higher and lower frequencies to be combined, then we multiply their phase differences (expressed in lengths) with the factor $f_h^2 f_l^2/(f_h^2-f_l^2)$ to obtain TEC. This factor becomes smaller (TEC data become less noisy) if the two frequencies are more different. The actual values of this factor are 7.76, 9.52, and 42.08 for the L1–L5, L1–L2, and L2–L5 combinations, i.e., the L1–L5/L2–L5 combinations would have the smallest/largest noises.

Figure 7a compares slant TEC time series obtained with the same station–satellite pair (2007 – J07) using the three different phase combinations. Indeed, the L2–L5 combination shows the largest noise, and the L1–L5 combination shows a slightly smaller noise than the conventional L1–L2 combination. The total standard deviation (σ_{tot}) would be composed of real ionospheric TEC changes (σ_{ion}), caused, e.g., by small-scale electron density irregularities (scintillations), and phase reading errors within GNSS receivers (σ_{rx}). The latter would be enhanced by the frequency factor F as discussed above while the former would remain the same for any frequency combinations. Then, their variances would have the following relationship:

$$\sigma_{tot^2} = \sigma_{ion^2} + F^2\sigma_{rx^2} \qquad F \equiv f_{h^2} f_{1^2} / (f_{h^2} - f_{1^2}). \tag{1}$$

Figure 7b compares the total standard deviation σ_{tot} as a function of the factor F. We used (1) as the observation equation and estimated the two quantities σ_{ion} and σ_{rx} for three different periods by the least-squares method. Figure 7c indicates that the receiver noise σ_{rx} remains constant for the three periods while ionospheric scintillation

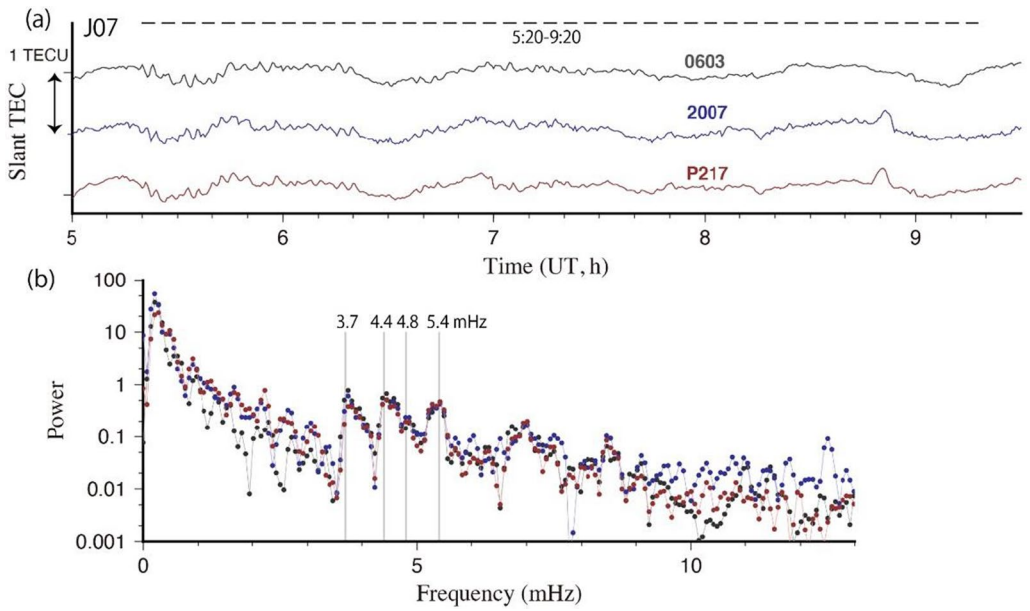

Fig. 5 **a** High-pass filtered slant TEC time series at three stations observed using J07, the QZSS geostationary satellite, at three GNSS stations 0603, 2007, and P217 (Fig. 1b). Frequency components of the 4-h data 5:20–9:20 UT (shown with a dashed line) obtained using the Blackman–Tukey method are shown in (**b**). We see three strong peaks (3.7, 4.4, and 5.4 mHz) and one weaker peak (4.8 mHz) for the TEC data at all the three stations (colors correspond to those in (**a**)

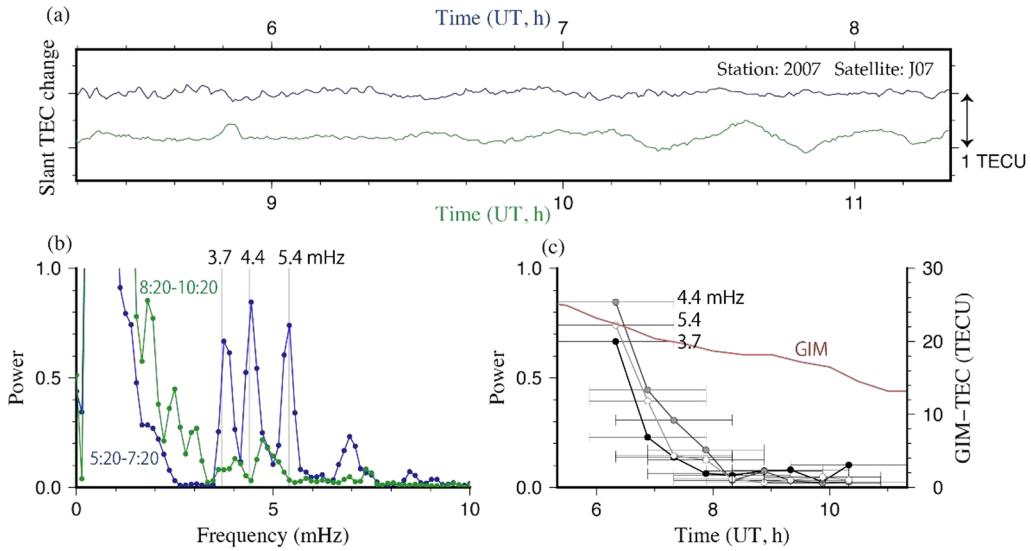

Fig. 6 **a** High-pass filtered slant TEC time series 5:20–8:20 (blue) and 8:20–11:20 (green) UT, at the 2007 station observed using J07 satellite. **b** Frequency components of the 2-h data 5:20–7:20 UT and 8:20–10:20 UT indicate that the peak powers mostly decayed in the second time window. **c** We select the three strong peaks (3.7, 4.4, and 5.4 mHz) and compare their powers obtained from a 2-h time window moving with a 1-h time step (horizontal bars indicate the periods representing the frequency spectra). The red curve in **c** indicates gentle afternoon decrease of vertical TEC above the volcano from GIM

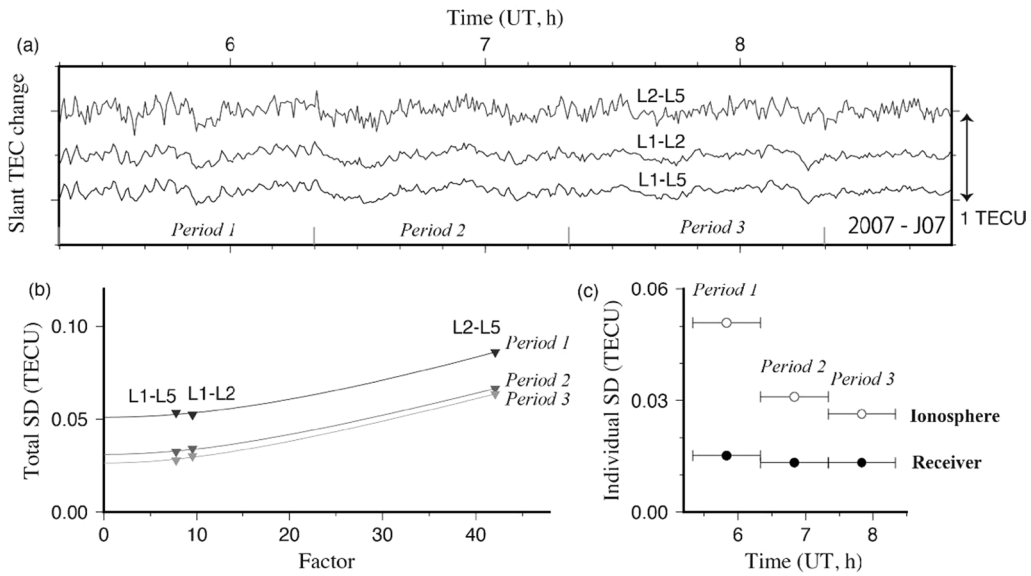

Fig. 7 **a** High-pass filtered slant TEC time series5:20–8:50 at the 2007 station observed using J07 satellite calculated with three different combinations of L1, L2, and L5 carrier phases. **b** Standard deviations of slant TEC σ_{tot} obtained by the three combinations as a function of the frequency factor F in Eq. (1). Three curves correspond to Period 1 (5:20–6:20), Period 2 (6:20–7:20) and Period 3 (7:20–8:20). **c** Receiver noises σ_{rx} remain nearly constant, while ionospheric scintillation σ_{ion} decays rapidly with time. The receiver noise σ_{rx} is scaled with the frequency factor for the L1–L2 combination

σ_{ion} decays rapidly as time elapses. This provides an additional support for the decay of atmospheric modes within 3 hours (Fig. 6c).

TEC oscillation amplitudes

Cahyadi et al. (2020) compared the TEC oscillation amplitudes relative to the background vertical TEC from three eruption cases and suggested that they might

be proportional to the mass eruption rate (MER). The motions of electrons in the ionospheric F region are constrained in the direction of the ambient geomagnetic fields. This causes the directivity of ionospheric disturbances. They appear strongly on the equator side of the volcano, i.e., stronger disturbances emerge on the southern side in northern hemisphere (e.g., Heki 2006; Kundu et al. 2021), and northern side in southern hemisphere (Nakashima et al. 2016).

Figure 8a shows how such north–south asymmetry occurs using numerical simulation of upward propagation of atmospheric acoustic waves following Kundu et al. (2021). There, hypothetical line-of-sight with elevation angle 45° from two points assumed 270 km due south (Ps) and due north (Pn) are given with white lines. In Fig. 8b, c we compare slant TEC changes as viewed from the points Pn and Ps. Their amplitude differs by a factor of ~ 4, and the amplitude observed at 0603 using J07, calculated assuming real azimuth and elevation of J07 from 0603 (red curve in Fig. 8b), is similar to the point Pn case. We discuss waves close to the acoustic cut-off frequency, and a simple raytracing (Kundu et al. 2021) involves errors by neglecting gravitational restoring forces. Nevertheless, this factor ~ 4 is supported by the real north–south asymmetry observed in the 2003 Tokachi-oki earthquake (Heki and Ping 2005).

The current 0603-J07 slant TEC peak-to-peak amplitude of ~ 0.23 TECU becomes ~ 0.19 TECU in vertical TEC by multiplying with the cosine of the incidence angle of line-of-sight (~ 33°) with the F region ionosphere. This corresponds to ~ 0.76% of the background vertical TEC, ~ 25 TECU according to GIM.

This relative TEC oscillation amplitude in the 2021 Fukutoku-Okanoba eruption is comparable to those associated with the 2015 Calbuco and 2010 Merapi eruptions (Cahyadi et al. 2020). However, we would have observed ~ 4 times as strong oscillation if we had a GNSS station to the south of the volcano (Fig. 8). If we consider a factor 4 difference, the TEC oscillation amplitude of the 2021 Fukutoku-Okanoba eruption may reach ~ 3% of the background vertical TEC, which exceeds the value for the 2014 Kelud eruption (Nakashima et al. 2016; Cahyadi et al. 2020). Then, the MER at the peak time (~ 5:20 UT) of the TEC oscillation may have been as large as 5×10^7 kg s^{-1}. This is consistent with the total amount

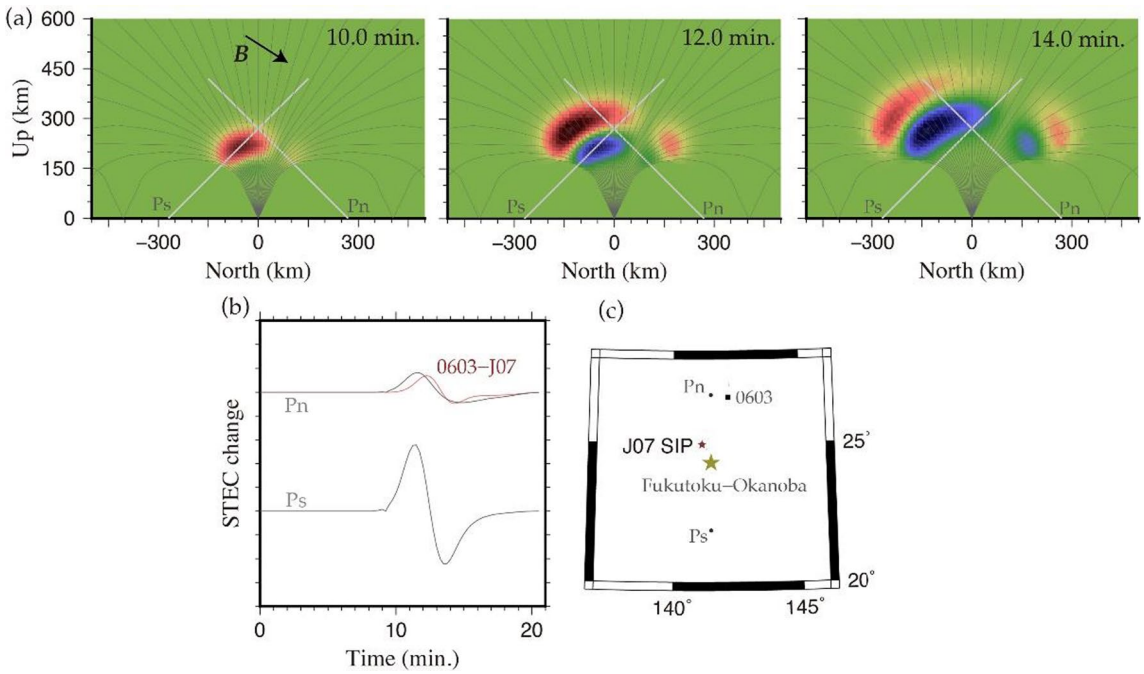

Fig. 8 **a** Numerical simulation of the upward propagation of atmospheric acoustic waves and ionospheric electron density anomalies made by the passage of the wave. Red and blue parts show the positive and negative electron density anomalies (arbitrary unit) in the north–south vertical section. We assumed a simple N-shaped pulse with a period of 4 min. Geomagnetic field (Inclination: 34.5°, Declination −3.0°, at a point ~ 300 km above Fukutoku-Okanoba, shown as makes north–south asymmetry. Details of the simulation are described in Kundu et al. (2021). In **b** we compare slant TEC signatures to be obtained by observing a satellite in the northern/southern skies, with elevation 45°, from hypothetical southern/northern points Ps/Pn (gray curves), and those assuming the real geometry of 0603-J07 (red curve). Unit is arbitrary and only relative amplitudes are meaningful. **c** Line-of-sight from 0603 to J07 extends almost southward with the similar elevation, the situation similar to the case for the point Pn

of ejecta in this eruption inferred as $3–10 \times 10^{11}$ kg (GSJ 2021).

Conclusions

We summarize this study as follows:

1. The 2021 August eruption of the Fukutoku-Okanoba submarine volcano caused typical ionospheric signatures associated with Plinian eruptions.
2. Atmospheric modes in four different frequencies are observed and the TEC oscillation decayed within 3 hours.
3. QZSS has two benefits for ionospheric studies, i.e., long continuous records suitable for frequency spectrum analyses, and three different microwave carriers that enable separation of intensities of true ionospheric scintillation signals from receiver noises.

Abbreviations

GEONET: GNSS Earth Observation Network; GNSS: Global Navigation Satellite System; GIM: Global ionospheric map; GLONASS: Global Orbiting Navigation Satellite System; GPS: Global Positioning System; GSI: Geospatial Information Authority of Japan; GSJ: Geological Survey of Japan; JMA: Japan Meteorological Agency; MER: Mass eruption rate; QZSS: Quasi-Zenith Satellite System; SD: Standard deviation; SIP: Sub-ionospheric point; TEC: Total electron content; TECU: TEC unit; UT: Universal time; VEI: Volcanic explosivity index.

Acknowledgements

We thank GSI for GNSS data. Constructive reviews by two anonymous referees improved the manuscript.

Authors' contributions

KH: conceptualization, data analysis, writing. TF: calculation related to L1, L2, and L5 combinations. All authors read and approved the final manuscript.

Authors' information

Kosuke Heki is a professor in Department of Natural History Sciences, Hokkaido University, Japan. He studies space geodesy, with strong interest in atmospheric sensing with GNSS. He pioneered various applications of GNSS-TEC including ionospheric disturbances immediately before and after large earthquakes.Tatsuya Fujimoto is a master course graduate student in Department of Natural History Sciences, Graduate School of Science, Hokkaido University. He is mainly interested in GNSS-TEC applications for studying sporadic-E irregularities.

Funding

This research was supported by JSPS KAKENHI Grant number JP20K04120.

Availability of data and materials

GEONET data can be downloaded from GSI ftp server (terras.gsi.go.jp) after a simple registration procedure. Most of the software systems used in this study can be found in the web page of the corresponding author (www.ep.sci.hokudai.ac.jp/~heki/software.htm).

Declarations

Competing interests

The authors declare that they have no known competing financial interests or personal relationships that could have appeared to influence the work reported in this paper.

Received: 21 December 2021 Accepted: 26 January 2022
Published online: 09 February 2022

References

Blanc E (1985) Observations in the upper atmosphere of infrasonic waves from natural or artificial sources—a summary. Annales Geophysicae, vol 3. European Geophysical Society, Katlenburg-Lindau, pp 673–687
Cahyadi MN, Rahayu RW, Heki K, Nakashima Y (2020) Harmonic ionospheric oscillation by the 2010 eruption of the Merapi volcano, Indonesia, and the relevance of its amplitude to the mass eruption rate. J Volcanol Geotherm Res 405:107047. https://doi.org/10.1016/j.jvolgeores.2020.107047
Cahyadi MN, Handoko EY, Rahayu RW, Heki K (2021) Comparison of volcanic explosions in Japan using impulsive ionospheric disturbances. Earth Planets Space 73:228. https://doi.org/10.1186/s40623-021001539-5
GSJ (2021) Fukutoku-Oka-no-Ba submarine volcano information, Geological Survey of Japan. www.gsj.jp/hazards/volcano/fukutokuokanoba/2021/index.html
Heki K (2006) Explosion energy of the 2004 eruption of the Asama Volcano, central Japan, inferred from ionospheric disturbances. Geophys Res Lett 33:L14303. https://doi.org/10.1029/2006GL026249
Heki K (2021) Chapter 21: Ionospheric disturbances related to earthquakes. Ionospheric dynamics and applications, geophysical monograph 260. Wiley, New York, pp 511–526. https://doi.org/10.1002/9781119815617.ch21
Heki K, Ping J-S (2005) Directivity and apparent velocity of the coseismic ionospheric disturbances observed with a dense GPS array. Earth Planet Sci Lett 236:845–855
JMA (2021) Volcanic activity of Fukutoku-Okanoba information on volcanic activities in 2021 August. www.data.jma.go.jp/svd/vois/data/tokyo/STOCK/monthly_v-act_doc/tokyo/21m08/331_21m08.pdf. Accessed August 2021
Kanamori H, Mori J (1992) Harmonic excitation of mantle Rayleigh waves by the 1991 eruption of Mount Pinatubo Philippines. Geophys Res Lett 19(7):721–724. https://doi.org/10.1029/92GL00258/full
Kundu B, Senapati B, Matsushita A, Heki K (2021) Atmospheric wave energy of the 2020 August 4 explosion in Beirut, Lebanon, from ionospheric disturbances. Sci Rep 11:2793. https://doi.org/10.1038/s41598-021-82355-5
Maeda J, Heki K (2015) Morphology and dynamics of daytime mid-latitude sporadic-E patches revealed by GPS total electron content observations in Japan. Earth Planets Space 67:89. https://doi.org/10.1186/s40623-015-0257-4
Mannucci AJ, Wilson BD, Yuan DN, Ho CH, Lindqwister UJ, Runge TF (1998) A global mapping technique for GPS-derived ionospheric total electron content measurements. Radio Sci 33:565–582. https://doi.org/10.1029/97RS02707
Nakashima Y, Heki K, Takeo A, Cahyadi MN, Aditiya A, Yoshizawa K (2016) Atmospheric resonant oscillations by the 2014 eruption of the Kelud volcano, Indonesia, observed with the ionospheric total electron contents and seismic signals. Earth Planet Sci Lett 434:112–116. https://doi.org/10.1016/j.epsl.2015.11.029
Nishida K, Kobayashi N, Fukao Y (2000) Resonant oscillation between the solid earth and the atmosphere. Science 287:2244–2246
Shestakov N, Orlyakovskiy A, Perevalova N, Titkov N, Chebrov D, Ohzono M, Takahashi H (2021) Investigation of ionospheric response to June 2009 Sarychev peak volcano eruption. Remote Sens 13:648. https://doi.org/10.3390/rs13040638
Watada S, Kanamori H (2010) Acoustic resonant oscillations between the atmosphere and the solid earth during the 1991 Mt Pinatubo eruption. J Geophys Res 115:B12319. https://doi.org/10.1029/2010JB007747

Publisher's Note